Structural elements that underlie Doc2β function during asynchronous synaptic transmission

Renhao Xue[1], Jon D. Gaffaney[1], and Edwin R. Chapman[2]

Department of Neuroscience, University of Wisconsin, Madison, WI 53706; and Howard Hughes Medical Institute, University of Wisconsin, Madison, WI 53706

Edited by Timothy A. Ryan, Weill Cornell Medical College, New York, NY, and accepted by the Editorial Board June 29, 2015 (received for review February 3, 2015)

Double C2-like domain-containing proteins alpha and beta (Doc2α and Doc2β) are tandem C2-domain proteins proposed to function as Ca^{2+} sensors for asynchronous neurotransmitter release. Here, we systematically analyze each of the negatively charged residues that mediate binding of Ca^{2+} to the β isoform. The Ca^{2+} ligands in the C2A domain were dispensable for Ca^{2+}-dependent translocation to the plasma membrane, with one exception: neutralization of D220 resulted in constitutive translocation. In contrast, three of the five Ca^{2+} ligands in the C2B domain are required for translocation. Importantly, translocation was correlated with the ability of the mutants to enhance asynchronous release when overexpressed in neurons. Finally, replacement of specific Ca^{2+}/lipid-binding loops of synaptotagmin 1, a Ca^{2+} sensor for synchronous release, with corresponding loops from Doc2β, resulted in chimeras that yielded slower kinetics in vitro and slower excitatory postsynaptic current decays in neurons. Together, these data reveal the key determinants of Doc2β that underlie its function during the slow phase of synaptic transmission.

asynchronous synaptic transmission | C2-domain | Ca^{2+} sensor | Doc2β | synaptotagmin 1

Ca^{2+}-triggered synaptic vesicle (SV) exocytosis in nerve terminals is often a biphasic process consisting of a fast, synchronous phase, occurring within milliseconds of Ca^{2+} influx, and a slow, asynchronous phase, which can persist for hundreds of milliseconds. Synaptotagmin 1 (syt1) is thought to function as a Ca^{2+} sensor for the rapid phase of release (1–4). Although syt1-KO neurons display a complete loss of synchronous transmission, the asynchronous component persists (5–7), suggesting that distinct Ca^{2+} sensors regulate these processes.

Recently, a specific subset of membrane-trafficking proteins has been proposed to mediate asynchronous release selectively (8, 9), including another member of the syt family of Ca^{2+} sensors, syt7 (10). Syt7 is unique in that it has the slowest intrinsic kinetics of all syt isoforms (11), so it is well suited to drive the slow phase of transmission. However, in mouse neurons, loss of syt7 has no effect on the decay kinetics of single evoked synaptic currents (10, 12–14); rather, syt7-KO neurons exhibited a reduction in synaptic vesicle replenishment (13). The double C2-domain (Doc2) proteins, which also exhibit slow kinetics in vitro, are Ca^{2+}-binding proteins required for normal levels of asynchronous release in hippocampal neurons (15, 16). However, whether Doc2 proteins function as Ca^{2+} sensors that directly regulate slow transmission remains an open issue, as detailed further below.

To date, three isoforms of Doc2 have been identified: α, β, and γ. Doc2α is expressed only in brain (17), while Doc2β and γ are expressed in a variety of tissues, including the brain (18, 19); γ does not appear to sense Ca^{2+} (19). During asynchronous transmission, Doc2 α and β are able to substitute for one another functionally (15), and because Doc2β can be generated more readily in bacteria, the current study is focused on this isoform. Under resting conditions, Doc2β is a cytosolic protein. Upon depolarization of neurons and neuroendocrine cells, increases in intracellular Ca^{2+} ($[Ca^{2+}]_i$) drive the rapid translocation of Doc2β to the plasma membrane (20, 21). In addition, stimulation of adipocytes with insulin and pancreatic B cells with glucose also trigger translocation of Doc2β to the plasma membrane (22, 23). These findings are consistent with the idea that Doc2β functions as a Ca^{2+} sensor for secretion, because it must be present at release sites to regulate exocytosis.

Several observations suggest that Doc2β regulates asynchronous synaptic transmission. First, Ca^{2+} enhances the binding of Doc2β to negatively charged phospholipids (i.e., phosphatidylserine and phosphatidylinositol 4,5-bisphosphate) (16, 24, 25) and to soluble NSF attachment protein receptor proteins (SNAREs) (23–25) to accelerate membrane fusion in vitro (15, 16, 26). Second, Doc2β displays membrane disassembly kinetics (k_{diss}) upon chelation of Ca^{2+}, consistent with time scales observed for asynchronous release (15). Finally, altering the expression levels of Doc2β in neuronal cultures changes the relative proportion of asynchronous and synchronous release (15). However, a Doc2β mutant that lacks any apparent Ca^{2+}-binding activity yields enhanced asynchronous release when overexpressed in syt1-KO neurons, confounding the interpretation that Doc2β is a Ca^{2+} sensor for SV exocytosis (15, 16).

Similar to the cytoplasmic domain of syt1, Doc2β is composed largely of tandem C2 domains (C2A and C2B). Crystal structures of each C2 domain of Doc2β have been reported (27), and they conform to the same overall structure reported for other C2 domains that bind Ca^{2+}. Namely, five acidic amino acid side chains coordinate Ca^{2+} ions in two loops near the tip of each domain: in C2A, loop 1 (amino acids 152–163) and loop 3

Significance

Evoked synaptic transmission is mediated by synchronous and asynchronous phases of neurotransmitter release. Synaptotagmin 1 (syt1) serves as the Ca^{2+} sensor for synchronous release. Recently, we proposed that double C2-like domain-containing protein alpha and beta (Doc2α and Doc2β), cytosolic proteins with tandem C2 domains homologous to syt1, function as Ca^{2+} sensors for asynchronous release, but this idea remains controversial. Here, we systematically analyzed the functional significance of each Ca^{2+} ligand in Doc2β and found a correlation between the Ca^{2+}-dependent translocation activity of these mutants (to the plasma membrane) and changes in asynchronous release. Moreover, we show that syt1–Doc2β chimeras exhibit altered kinetics in vitro and change the rates of synaptic transmission in cultured neurons. These results establish Doc2β as a Ca^{2+} sensor for the slow phase of neurotransmission.

Author contributions: R.X., J.D.G., and E.R.C. designed experiments; R.X. and J.D.G. performed experiments; R.X., J.D.G., and E.R.C. analyzed data; and R.X., J.D.G., and E.R.C. wrote the paper.

The authors declare no conflict of interest.

This article is a PNAS Direct Submission. T.A.R. is a guest editor invited by the Editorial Board.

[1]R.X. and J.D.G. contributed equally to this work.

[2]To whom correspondence should be addressed. Email: chapman@wisc.edu.

This article contains supporting information online at www.pnas.org/lookup/suppl/doi:10.1073/pnas.1502288112/-/DCSupplemental.

(amino acids 218–226); in C2B, loop 4 (amino acids 291–303) and loop 6 (amino acids 356–365) (Fig. 1*A*). Also, from biochemical experiments, it is well established that the isolated C2B domain of Doc2β binds Ca^{2+}, and this interaction triggers both robust binding to acidic phospholipids in vitro (16) and translocation to the plasma membrane of cells (23, 27). The ability of C2A to sense Ca^{2+} is more complicated; the isolated domain does not exhibit detectable Ca^{2+}-binding activity (16, 27), but it efficiently binds acidic phospholipids in response to Ca^{2+} (16, 18, 24). Isolated C2A also failed to translocate to the plasma membrane of PC12 cells following depolarization; however, translocation was achieved using a Ca^{2+} ionophore to increase $[Ca^{2+}]_i$ further (27).

In previous studies, Ca^{2+} ligands in loop 3 (D218 and D220) and loop 6 (D357 and D359) of Doc2β were neutralized via substitution with aspargine (15, 16); these positions were selected because analogous mutations have been shown to abolish the Ca^{2+}-dependent membrane-binding activity of the C2 domains of syt1 (28, 29). However, the loop-3 mutations resulted in the anomalous constitutive plasma membrane localization of Doc2β in chromaffin and PC12 cells (16, 21, 24), whereas the loop-6 mutations had no effect on translocation. In sharp contrast, neutralization of acidic residues in loops 1 and 4 of Doc2β abolish translocation to the plasmalemma in adipocytes (23). At present, a systematic analysis of each Ca^{2+} ligand has not been reported.

In the current study, we first identified structural elements of Doc2β that mediate Ca^{2+}-triggered translocation. We found that these same elements, which lie mainly in the C2B domain, also mediate the effects of Doc2β on asynchronous synaptic transmission. In the C2A domain, these mutations either had no effect or resulted in the constitutive activation of the protein, depending on which acidic Ca^{2+} ligands were neutralized. These results aid interpretation of earlier mutagenesis studies and support a model in which Doc2β functions as a Ca^{2+} sensor for the slow phase of synaptic transmission.

Results

Structural Elements That Mediate Translocation of Doc2β. What are the structural elements within the tandem C2 domains of Doc2β that mediate translocation? As described above, simultaneous neutralization of Ca^{2+} ligands in loops 1 and 4 of Doc2β

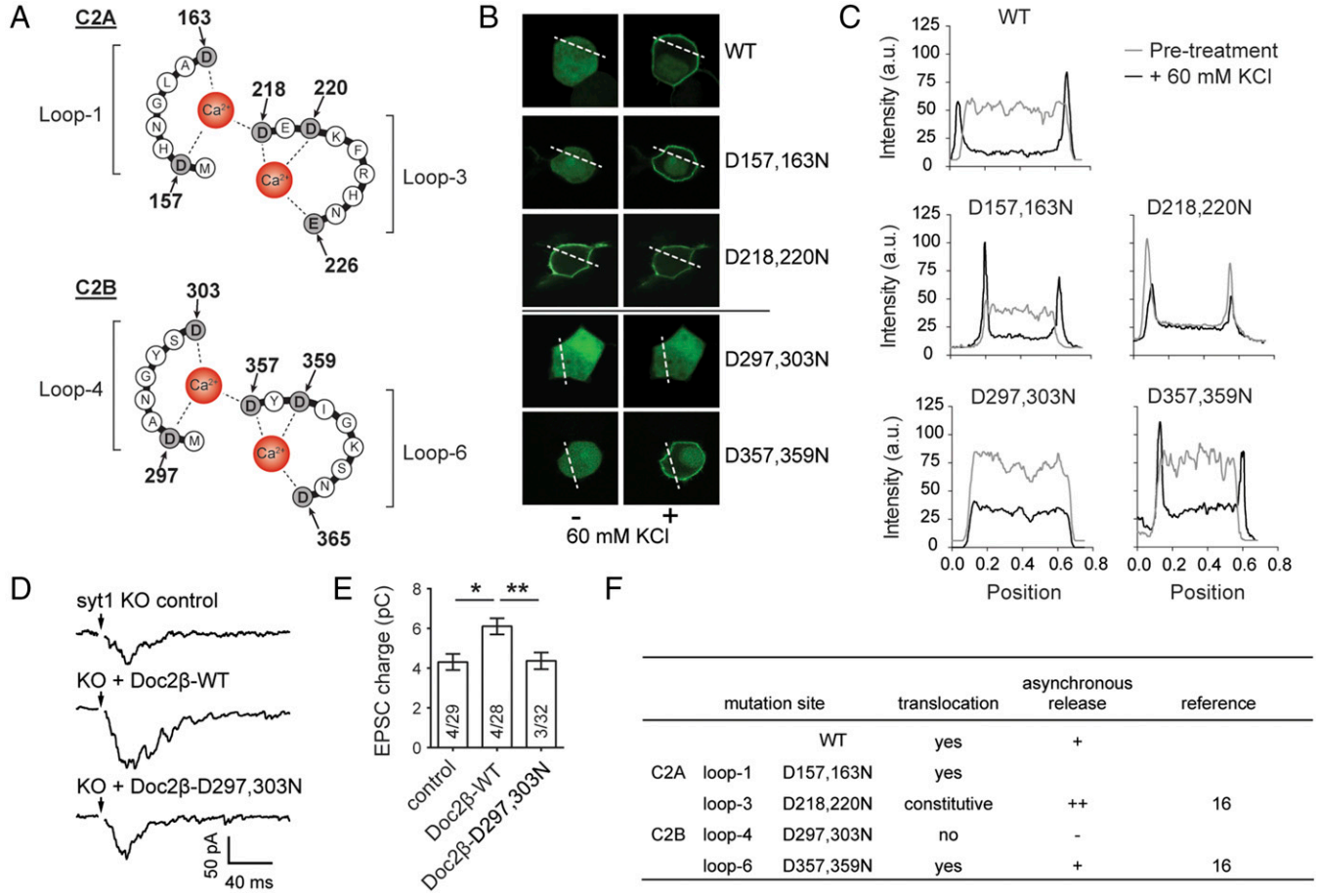

	mutation site		translocation	asynchronous release	reference
		WT	yes	+	
C2A	loop-1	D157,163N	yes		
	loop-3	D218,220N	constitutive	++	16
C2B	loop-4	D297,303N	no	-	
	loop-6	D357,359N	yes	+	16

Fig. 1. Disruption of the individual Ca^{2+}-binding loops of Doc2β: effects on translocation and asynchronous release. (*A*) A schematic diagram showing the Ca^{2+}-binding loops in the C2A and C2B domains of Doc2β and the residues predicted to coordinate Ca^{2+} ions. Two Ca^{2+} ligands in each loop (gray) were neutralized by replacing Asp with Asn. (*B*) WT and mutant forms of Doc2β were fused to GFP and expressed in PC12 cells, and their abilities to translocate to the plasma membrane upon depolarization with 60 mM KCl was monitored by confocal microscopy. (*C*) Representative line scans of GFP fluorescence (dotted white lines in *B*) from PC12 cells before and after depolarization with KCl; quantitative analysis of these scans is provided in Fig. S2. a.u., arbitrary units. (*D*) Representative evoked EPSC recordings from syt1-KO hippocampal neurons expressing either WT or the D297,303N mutant form of Doc2β; results from the D218,220N and D357,359N mutant forms of Doc2β were published previously (16). (*E*) The total charge transfer from syt1-KO neurons (4.31 ± 0.41 pC, $n = 29$) was increased by the expression of the WT (6.11 ± 0.41 pC, $n = 28$) but not the D297,303N mutant (4.37 ± 0.42 pC, $n = 32$) form of Doc2β. Data are presented as mean ± SEM; $*P < 0.05$, $**P < 0.01$, Kolmogorov–Smirnov test. The number of animals, *N*, and the number of cells, *n*, are indicated in the bar graph as *N*/*n*. (*F*) Summary of the translocation and asynchronous release data for WT Doc2β and the tandem Ca^{2+}-ligand mutants. +, ~50% increase; ++, ≥100% increase; –, no significant increase.

abolished Ca^{2+}-dependent membrane translocation in adipocytes (23). Analogous mutations in both loop 3 and 6 eliminated Ca^{2+}-dependent phospholipid-binding activity in vitro but gave rise to constitutive localization at the plasma membrane of PC12 cells (16), so these elements remain unclear. To define the structural determinants that underlie translocation, we disrupted the Ca^{2+}-binding activity of individual loops by mutating two acidic Ca^{2+} ligands within each loop (note: each loop has two or three acidic ligands; Fig. 1*A*) and tested these mutants in the same experimental system.

We first determined the Ca^{2+} sensitivity of each mutant by measuring the $[Ca^{2+}]_{1/2}$ for membrane binding via cosedimentation with artificial liposomes (Fig. S1). Mutations in loop 1 (D157,163N) or loop 3 (D218,220N) had no significant effect on the Ca^{2+} dependence for membrane binding, whereas loop 4 (D297,303N) and loop 6 (D357,359N) displayed more than a fourfold increase in the $[Ca^{2+}]_{1/2}$ value, compared with WT. The quadruple mutant D157,163,297,303N failed to bind liposomes in the presence or absence of Ca^{2+}, as did the D218,220,357,359N mutant that we described previously (16).

The double mutants then were tested for their ability to translocate to the plasma membrane of PC12 cells following depolarization with 60 mM KCl (Fig. 1 *B* and *C*; quantified in Fig. S2). WT Doc2β readily translocates from the cytosol to the plasma membrane (16, 20, 21). Consistent with the liposome-binding experiments above, simultaneous neutralization of both acidic ligands in C2A loop 1 (D157,163N) had no effect on translocation activity. As observed previously, neutralization of two ligands in loop 3 (D218,220N) resulted in constitutive binding to the plasma membrane (16, 21, 24). Interestingly, this mutation does not significantly alter the $[Ca^{2+}]_{1/2}$ for lipid binding, consistent with the idea that the localization at the plasma membrane occurs via a Ca^{2+}-independent mechanism [i.e., in our hands, this mutation does not convert Doc2β to a higher-affinity Ca^{2+} sensor (16), as proposed previously (21)].

Analogous experiments focused on the C2B domain yielded different results. Neutralization of both Ca^{2+} ligands (D297,303N) in loop 4 of the C2B domain (analogous to loop 1 in C2A) completely disrupted Ca^{2+}-dependent translocation, and neutralization of two ligands (D357,359N) in loop 6 (analogous to loop 3 in C2A) had no discernable effect (16). Apparently, the $[Ca^{2+}]_i$ that is achieved during depolarization of PC12 cells is sufficient to drive translocation of the loop-6 mutant but not the loop-4 mutant. Together, these findings highlight striking differences between the functional properties of the tandem C2 domains of Doc2β and support the idea that the Ca^{2+}-sensing activity of C2B, particularly within loop 4, is crucial for translocation.

Membrane Translocation of Doc2β Correlates with Enhanced Asynchronous Release. To determine whether the membrane translocation activity of Doc2β is functionally related to asynchronous synaptic transmission, we analyzed the effect of mutant forms of the protein on evoked excitatory postsynaptic currents (EPSCs) recorded from hippocampal neurons cultured from syt1-KO mice. Syt1-KO neurons, which lack the synchronous component of transmission, were used to simplify analysis of the asynchronous component of release. Consistent with a previous report, expression of WT Doc2β enhanced asynchronous release (Fig. 1*D* and figures 1 and 4 in ref. 16). Earlier work showed that the D218,220N mutant yielded the largest increase in asynchronous release among all of the constructs tested thus far and that this mutant is constitutively associated with the plasma membrane (figures 4 and 6 in ref. 16). However, neurons expressing the D297,303N mutant, which fails to translocate (Fig. 1 *B* and *C*), had no effect on asynchronous release (Fig. 1*E*). Moreover, tandem mutations in loop 6 (D357,359N) did not impair the ability of Doc2β to enhance asynchronous release or to translocate (figures 4 and 6 in ref. 16). Together, these data reveal that translocation activity correlates with the ability of Doc2β to regulate asynchronous release in neurons (Fig. 1*F*).

Next, we extended our analysis to the individual Ca^{2+} ligands in each C2 domain of Doc2β. Each of the five acidic amino acid residues in the C2A domain that coordinate Ca^{2+} were neutralized independently by substitution with an asparagine. None of these mutations altered the Ca^{2+} dependence for binding to artificial liposomes (Fig. S3). Substitution of four of the five acidic residues in the C2A domain had no effect on the translocation activity, but neutralization of one residue, D220N, resulted in the anomalous constitutive plasma membrane localization observed for the D218,220N mutant as described above. Because the D218,220N and D220N mutants had WT $[Ca^{2+}]_{1/2}$ values for binding to artificial liposomes, these results indicate the presence of additional effectors in cells that are not recapitulated by the synthetic membranes (i.e., proteins or rare or labile lipids). With the exception of the anomalous D220N mutation, these results further demonstrate that the Ca^{2+}-binding activity of the C2A domain is dispensable for translocation in cells.

In sharp contrast to our findings regarding C2A, neutralization of three of the five acidic Ca^{2+} ligands in the C2B domain (D297N, D303N, and D357N) displayed increases in the $[Ca^{2+}]_{1/2}$ for binding to liposomes (Fig. S3 *B* and *C*). Consistent with the cosedimentation experiments, only these three mutations disrupted translocation activity (Fig. 2 *A* and *B* and quantified in Fig. S2); the other two mutations had no discernable effect. Together, these findings confirm that the C2B domain of Doc2β functions as the Ca^{2+}-sensing module that mediates translocation.

To relate translocation to asynchronous synaptic transmission further, four Ca^{2+}-ligand point mutants with different translocation properties were overexpressed in cultured syt1-KO neurons, and their effects on EPSCs were characterized. D220N, which is constitutively bound to the plasmalemma, resulted in a significantly greater enhancement of asynchronous EPSCs than WT Doc2β (Fig. 2 *C* and *D*). The D303N mutant, which failed to translocate, did not enhance asynchronous neurotransmitter release. The D218N and D359N mutants exhibited normal translocation activity and enhanced asynchronous release to the same extent as the WT protein (Fig. 2*E*). Moreover, we confirmed that WT and two representative mutant forms of Doc2β (D218,220N and D297,303N) exhibited the same translocation activity in neurons as they did in PC12 cells (Fig. S4): The WT protein translocated in response to Ca^{2+} entry, D218,220N was constitutively bound to the plasma membrane, and D297,303N failed to translocate. Together, these experiments indicate that translocation of Doc2β plays a crucial role in asynchronous release and demonstrate that Doc2β must sense Ca^{2+} to regulate the slow component of transmission (unless constitutively activated by substituting D220).

Syt1–Doc2β Chimeras Exhibit Altered Kinetics in Vitro. The findings described above support the idea that Doc2β must bind Ca^{2+} to facilitate asynchronous transmission. In the next series of experiments, we determined whether the kinetics of release can be tuned by exchanging structural elements between Doc2β and a fast Ca^{2+} sensor for SV exocytosis, syt1.

We first generated a series of syt1–Doc2β chimeras and characterized the rate at which they disassemble from liposomes upon rapid mixing with excess Ca^{2+} chelator (11, 16). These kinetic experiments are intended to mimic the decay of Ca^{2+} transients in presynaptic boutons, thereby addressing the question of whether EPSC decay rates are determined, in part, by the rate at which the Ca^{2+} sensor for SV exocytosis releases a critical effector, membranes. Earlier work showed that both syt1 and Doc2β must interact with anionic phospholipids to drive fusion in vitro (15, 30), and a recent study indicates that syt1 must penetrate membranes to drive SV exocytosis in neurons (31).

Initially, the individual C2 domains were exchanged between syt1 and Doc2β to generate syt1 C2A-Doc2β C2B (SADB) and Doc2β C2A-syt1 C2B (DASB) chimeras. We note that stopped-flow

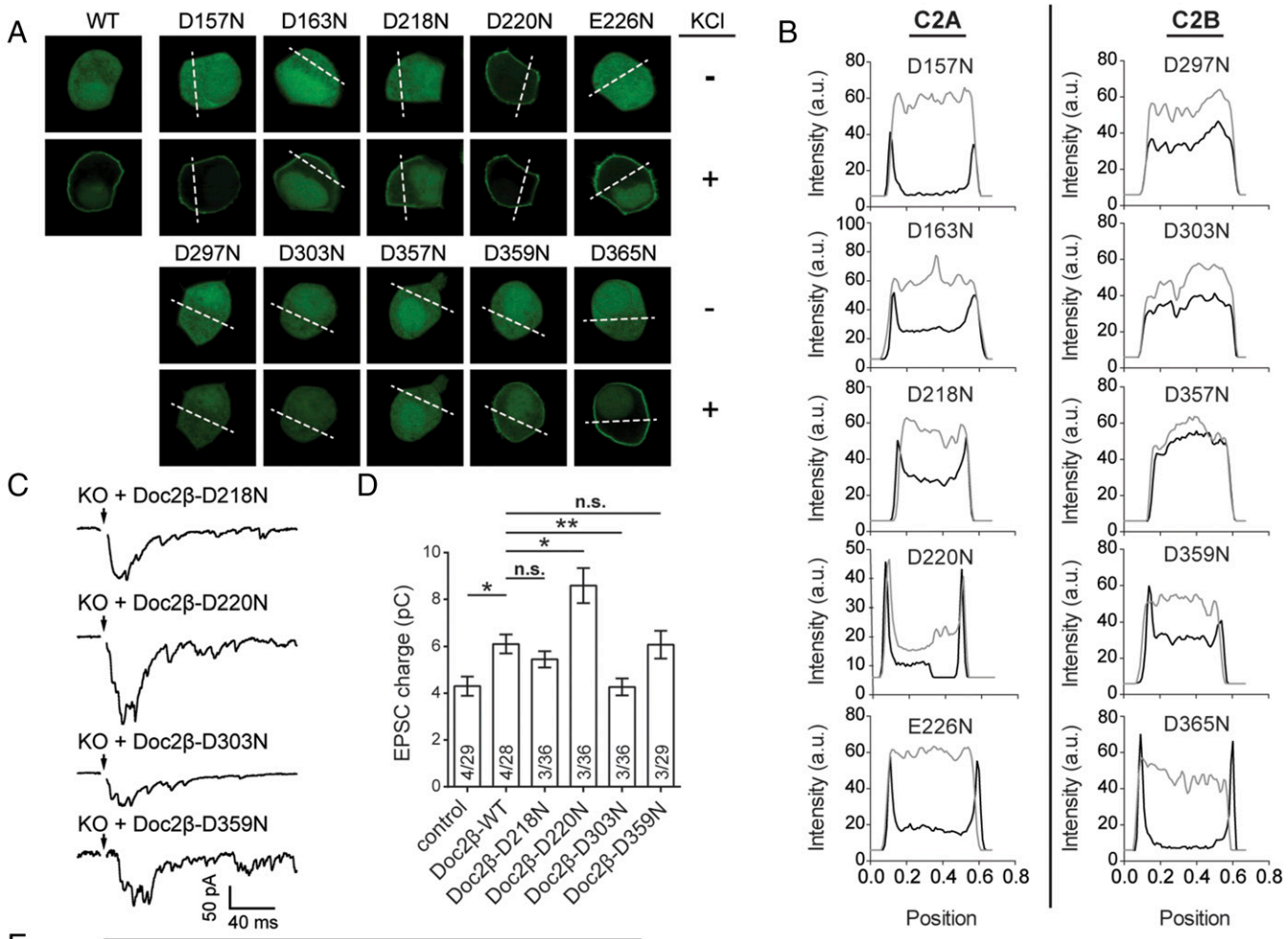

E

mutation site			translocation	asynchronous release
		WT	yes	+
C2A	loop-3	D218N	yes	+
		D220N	constitutive	++
C2B	loop-4	D303N	no	-
	loop-6	D359N	yes	+

Fig. 2. Neutralization of individual Ca^{2+} ligands in the C2B domain abolishes the ability of Doc2β to translocate to the plasma membrane and to drive asynchronous transmission. (*A*) Each of the acidic residues that coordinate Ca^{2+} in Doc2β (Fig. 1*A*) was individually replaced with Asn and expressed as a GFP-fusion protein in PC12 cells; translocation to the plasma membrane was monitored as in Fig. 1. (*B*) Representative line scans (dotted white lines in *A*) before and after depolarization with KCl; quantitative analysis of these scans is provided in Fig. S2. (*C*) Representative evoked EPSCs recorded from syt1-KO hippocampal neurons expressing D218N, D220N, D303N, or D359N mutant forms of Doc2β. (*D*) The expression of WT Doc2β enhanced the total charge transfer in syt1-KO neurons; the same results were observed for the D218N (5.45 ± 0.35 pC, $n = 36$) and D359N (6.08 ± 0.59 pC, $n = 29$) mutants. Interestingly, expression of Doc2β D220N, a mutant that is constitutively associated with the plasma membrane, yielded an even greater enhancement of the EPSC charge transfer (8.6 ± 0.75 pC, $n = 36$). In contrast, Doc2β D303N had no effect on total EPSC charge when expressed in syt1-KO neurons (4.27 ± 0.36, $n = 36$). Data are presented as mean ± SEM; n.s., not significant; $P > 0.05$, $^*P < 0.05$, $^{**}P < 0.01$, Kolmogorov–Smirnov test. The number of animals, *N*, and the number of cells, *n*, is indicated in the bar graph as *N*/*n*. (*E*) Summary of the translocation and asynchronous release results for WT and Ca^{2+}-ligand point mutant forms of Doc2β. +, ~50% increase; ++, >100% increase; –, no significant increase.

rapid-mixing studies of the isolated C2 domains of Doc2β revealed that both domains have slow membrane-disassembly kinetics (Fig. S5*A*), and so, as expected, both SADB and DASB chimeras displayed intermediate disassembly rates (k_{diss}) compared with syt1 or Doc2β C2AB domains (Fig. 3*A*). The syt1–Doc2β chimeras were refined by swapping individual Ca^{2+}- and membrane-binding loops of syt1 with the corresponding regions of Doc2β; these constructs are designated DL2–DL6 (Fig. 3*B*; note: loops 1, 3, 4, and 6 play key roles in coordinating Ca^{2+}; for completeness, loops 2 and 5 also were included in this analysis). We were unable to obtain sufficient quantities of recombinant syt1 DL1 C2AB, so this construct was not included in our in vitro studies. The kinetics of the syt1 DL2, DL3, and DL5 chimeras were indistinguishable from WT syt1 C2AB; however, the DL4 and DL6 mutants displayed significantly slower disassembly kinetics upon rapid mixing with EGTA (Fig. 3*C*).

Because syt1 and Doc2β might act, in part, by binding to target SNARES (t-SNAREs), we examined these interactions using a

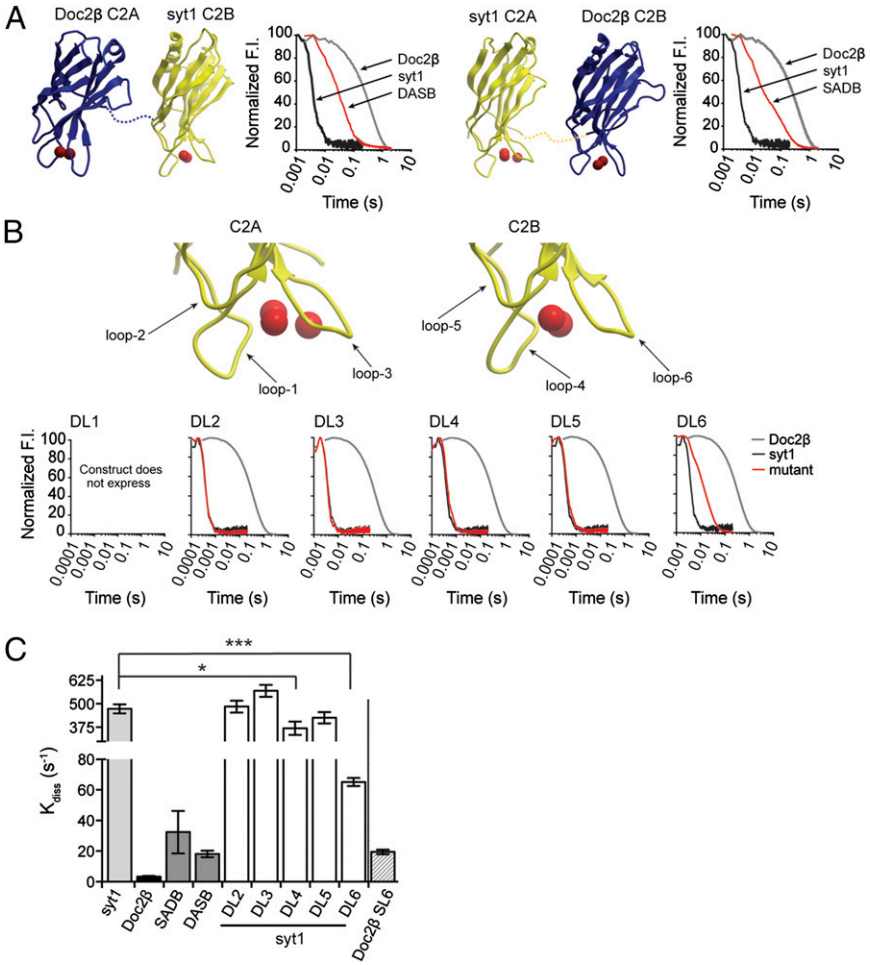

Fig. 3. Syt1–Doc2β chimeras reveal that the C2B domain largely determines the disassembly rate of Ca^{2+}•sensor•lipid complexes upon rapid chelation of Ca^{2+}. (*A*) Illustration of syt1–Doc2β chimeras. DASB, Doc2β C2A domain linked to the syt1 C2B domain; SADB, syt1 C2A domain linked to the Doc2β C2B domain. Representative models were created using the crystal structures of rat Doc2β [blue: C2A, Protein Data Bank (PDB) ID code 4LCV; C2B, PDB ID code 4LDC] and syt1 (yellow: C2A, PDB ID code 1BYN; C2B, PDB ID code 1K5W). Ca^{2+} ions are shown as red spheres. Liposomes that harbored dansyl-PE were incubated with 1 mM Ca^{2+} and with syt1 C2AB, Doc2β C2AB, or the indicated chimera. The protein•Ca^{2+}•lipid complexes were mixed rapidly with 5 mM EGTA, and the loss of FRET between endogenous Trp residues and the dansyl-labeled liposomes was measured as a function of time using a stopped-flow spectrometer. (*B*) The analysis in *A* was repeated for mutants in which individual syt1 Ca^{2+}-binding loops were replaced with the corresponding loop from Doc2β. (*C*) The k_{diss} values were determined by fitting the disassembly traces with single exponential functions and are plotted as the mean ± SEM; $^{***}P < 0.0001$, $^{*}P < 0.05$. Data are from more than five independent trials.

coflotation assay with syntaxin1A/SNAP-25B heterodimers reconstituted into proteoliposomes. All the chimeras bound t-SNAREs in a Ca^{2+}-dependent and stoichiometric manner, further establishing that each chimera is folded correctly (Fig. S6).

The DL6 mutant displayed the most robust changes in disassembly kinetics; therefore, we carried out additional mutagenesis within this structural element. Sequence alignment between loop 6 of syt1 and Doc2β revealed five amino acid differences. The differences in the positioning of these amino acids result from the insertion of a lysine residue (K366) in syt1. Each of these syt1 residues was replaced by the corresponding residues of Doc2β, individually or in pairs. In addition, the K366 residue was deleted to shift the position of each amino acid to correspond to Doc2β loop 6 (Fig. S5 *C* and *D*). No differences in membrane disassembly kinetics were observed among these mutants, suggesting that the entire loop is required to alter the kinetics of syt1 (Fig. S5). We also found that replacing Doc2β loop 6 with the corresponding loop from syt1 (Doc2β SL6) accelerated the membrane disassembly kinetics of Doc2β (Fig. 3*C*), further establishing the role of loop 6 in the disassembly kinetics of the lipid•protein•Ca^{2+} complex.

Tuning the Kinetics of Ca^{2+}-Dependent SV Release in Hippocampal Synapses. We next determined whether any of the syt1–Doc2β chimeras alter the kinetics of SV release in cultured hippocampal neurons. Full-length variants of the syt1 chimeras were generated (*Materials and Methods*) and expressed in syt1-KO neurons via lentiviral infection; again, syt1-KOs were used to simplify analysis, because the synchronous component of release is absent. WT syt1 or a construct composed of the C2AB domain of Doc2β fused to the luminal/transmembrane domain of syt1 (tm-Doc2β) (15) was used as control. All the chimeras were well expressed (Fig. S7) and properly targeted to synapses (Fig. 4 *A* and *B*).

To determine whether the mutants affected the number of vesicles available for release, the readily releasable pool (RRP) was measured under each condition, using hypotonic sucrose (7). Interestingly, all the chimeras except tm-Doc2β were able to completely restore the small RRP characteristic of syt1-KO neurons, back to WT levels (Fig. 4 *C* and *D*). These results indicate that either of the C2 domains in syt1 is sufficient to rescue the RRP. Because the size of the RRP was similar across conditions (i.e., for different chimeras), differences in evoked EPSC charge can be interpreted as an alteration in the SV-release step.

Evoked EPSCs were recorded from syt1-KO neurons expressing WT syt1, tm-Doc2β, tm-SADB, or tm-DASB (Fig. 5). As expected, full rescue of rapid transmission was observed using WT syt1, whereas the tm-Doc2β chimera gave rise to a modest increase in slow, asynchronous transmission, as reported previously (15). Interestingly, neurons expressing the tm-SADB and tm-DASB chimeras displayed intermediate kinetics: Both chimeras yielded slower rise times and decay kinetics compared with WT syt1, and these kinetics were faster than for tm-Doc2β. These data are consistent with the results from the stopped-flow experiments (Fig. 3). We note that the EPSC decay for the tm-SADB chimera was slightly but significantly slower than for the tm-DASB chimera (Fig. 5*D*), despite their similar membrane disassembly rates. This finding is consistent with the notion that the C2B domain plays a larger role than the C2A domain in the function of both Doc2β and syt1. However, tm-SADB drives SV release much less

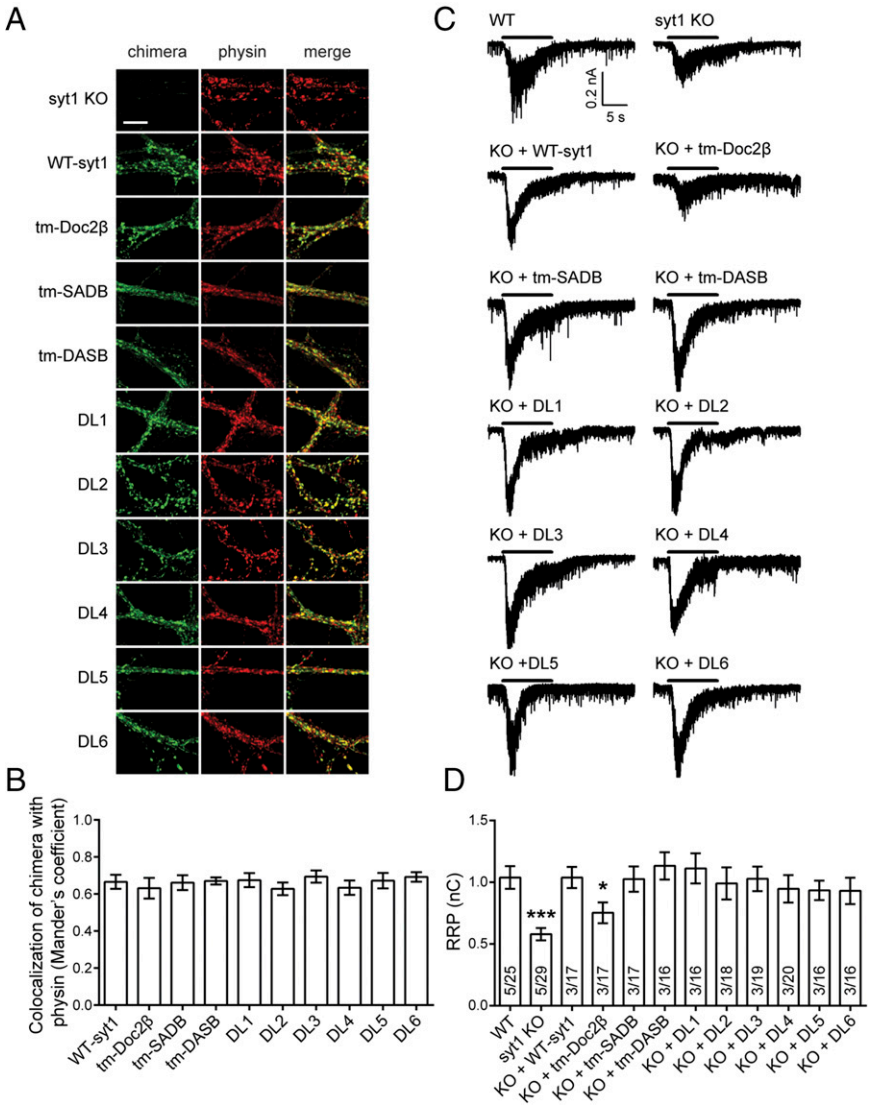

Fig. 4. Syt1–Doc2β chimeras are targeted to nerve terminals. (*A*) WT syt1 or full-length versions of the indicated syt1–Doc2β chimeras were expressed in syt1-KO hippocampal neurons by lentiviral infection. The infected neurons were imaged using confocal microscopy. (Scale bar, 10 μm.) (*B*) The extent of colocalization of WT syt1 or the syt1–Doc2β chimeras with synaptophysin (physin) was quantified by calculating the Mander's coefficient in each image. Six images from two independent litters of mice were analyzed for each condition. Data are presented as mean ± SEM. No significant differences were found using one-way ANOVA. (*C*) Representative EPSCs elicited with hypertonic sucrose, recorded from WT neurons, syt1-KO neurons, and syt1-KO neurons expressing the indicated chimera; black bars indicate local perfusion with 500 mM sucrose. (*D*) RRP size was quantified by integrating the total charge transfer during the application of sucrose. All the syt1–Doc2β chimeras fully rescued the diminished size of the RRP in the syt1-KO neurons, with the exception of tm-Doc2β. Data are presented as mean ± SEM; $*P < 0.05$, $**P < 0.01$ vs. WT, Kruskal–Wallis test followed by Dunn's post hoc test. The number of animals, *N*, and the number of cells, *n*, are indicated in the bar graph as *N*/*n*.

efficiently than tm-DASB, because it had only small effects on the amplitude and charge of the EPSCs (Fig. 5*D*). These data indicate tm-SADB is not a fully effective Ca^{2+} sensor when expressed in nerve terminals.

The syt1 DL1, DL2, DL3, and DL5 chimeras fully rescued fast-release kinetics in syt1-KO neurons (Fig. 6 *A* and *D*). However, expression of syt1 DL4 or DL6 only partially rescued the peak amplitude. Analysis of the kinetic parameters of these latter chimeras revealed significantly longer rise times and slower decay kinetics (Fig. 6*D*). The same trends were observed when EPSCs were recorded under more physiological conditions (35 °C, with 1.2 mM Ca^{2+} in the bath solution) (Fig. S8). Together, these data further establish the importance of the C2B domain of Doc2β.

We note that DL6 has a larger effect than DL4 on membrane disassembly kinetics in the stopped-flow rapid-mixing experiments. In cultured hippocampal neurons, however, expression of the DL4 chimera had a greater effect than the expression of DL6 on the kinetics of transmission. Perhaps this finding is not surprising: As detailed above, the artificial liposomes used in the in vitro experiments do not fully recapitulate the plasma membrane of living cells, because they lack proteins and a variety of low-abundance lipids.

To ensure that the altered EPSC kinetics (Figs. 5 and 6) were not the result of changes in postsynaptic AMPA receptors, miniature EPSCs (mEPSCs) were recorded from syt1-KO neurons expressing each chimera (Fig. S9). The amplitude, charge, and kinetics (20–80% rise time and 80–20% decay time) of individual mEPSCs were unchanged when native syt1 was replaced with any of the syt1–Doc2β chimeras (Fig. S9*B*).

Discussion

From this study, three major conclusions can be drawn. First, the C2B domain is the crucial Ca^{2+}-sensing module that mediates the ability of Doc2β to enhance asynchronous release; the Ca^{2+}-binding activity of the C2A domain is dispensable. Second, Doc2β must translocate to the plasma membrane to regulate asynchronous synaptic transmission. Third, syt1–Doc2β chimeras can alter the kinetics of SV exocytosis. Together, these results reveal structural elements of the SV release machinery that determine the time course of synaptic transmission and support a model in which the Ca^{2+}-binding isoforms of Doc2, α and β, function as slow Ca^{2+} sensors for the slow phase of SV exocytosis.

Disparate Effects of Ca^{2+} Ligand Mutations in Doc2β. To better understand the Ca^{2+}-sensing properties of Doc2β, we examined each of its acidic Ca^{2+} ligands. Neutralization of four of the five acidic residues that coordinate Ca^{2+} in C2A had no effect on translocation activity or the ability of Doc2β to enhance slow

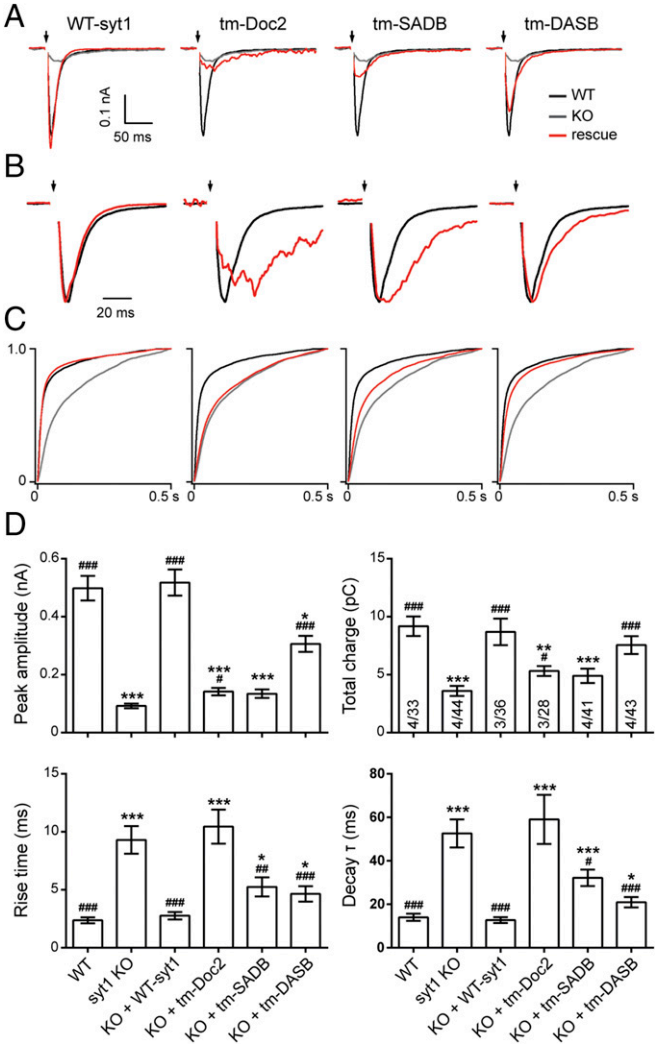

Fig. 5. Chimeras containing either C2 domain of Doc2β slow EPSC kinetics. (*A*) Averaged evoked EPSCs recorded from WT neurons (black traces), syt1-KO neurons (gray traces), and syt1-KO neurons expressing WT syt1 or the indicated syt1–Doc2β chimera (red traces). (*B*) The traces were normalized to the peak values. (*C*) The cumulative charge transfer functions were calculated from the EPSCs in *A*. (*D*) The peak amplitude, total charge, and 20–80% rise time (t_{rise}) were measured for each EPSC. The decay time (τ_{decay}) was calculated by exponential fitting of the decay phase of each EPSC. EPSC kinetics were slow in syt1-KO neurons (t_{rise} = 9.3 ± 1.19 ms, τ_{decay} = 52.58 ± 6.47 ms, n = 44) compared with WT neurons (t_{rise} = 2.37 ± 0.26 ms, τ_{decay} = 13.97 ± 1.63 ms, n = 33); this phenotype was rescued by WT syt1 (t_{rise} = 2.77 ± 0.32 ms, τ_{decay} = 12.7 ± 1.32 ms, n = 36) but not by tm-Doc2β (t_{rise} = 10.44 ± 1.46 ms, τ_{decay} = 59.02 ± 11.25 ms, n = 28). Replacing the C2A or C2B domain of syt1 with Doc2β resulted in significantly slower kinetics than in WT neurons (tm-DASB: t_{rise} = 4.64 ± 0.66 ms, τ_{decay} = 20.93 ± 2.39 ms, n = 43; tm-SADB: t_{rise} = 5.24 ± 0.82 ms, τ_{decay} = 32.18 ± 3.8 ms, n = 41), but these kinetics were faster than in syt1-KO neurons. Data are presented as mean ± SEM; $^{*}P < 0.05$, $^{**}P < 0.01$, $^{***}P < 0.001$ vs. WT, $^{\#}P < 0.05$, $^{\#\#}P < 0.01$, $^{\#\#\#}P < 0.001$ vs. syt1-KO, Kruskal–Wallis test followed by Dunn's post hoc test. The number of animals, *N*, and the number of cells, *n*, are indicated in the bar graph as *N*/*n*.

transmission when expressed in syt1-KO neurons. In sharp contrast, neutralization of the remaining ligand, D220, underlies the anomalous constitutive translocation of the Doc2β D218,220N double and D218,220,357,359N quadruple mutants reported previously (16, 21). The molecular mechanisms that underlie the unusual effects that result from mutating residue D220 are unknown; further structural studies are needed to address this issue. However, this result clarifies an earlier conundrum: The Doc2β quadruple Ca^{2+}-ligand mutant (D218,220,357,359N) does not bind Ca^{2+}, but it strongly increases asynchronous release, even more so than the WT protein, when overexpressed in neurons (15, 16). Detailed analysis revealed that this mutant enhances release, at least in part, by increasing the size of RRP (16); this unique property is not shared by WT Doc2β. These results highlight the complexity of Ca^{2+}-ligand mutations in C2 domains; in the case of position D220, mutations do not always simply disrupt Ca^{2+}-binding activity but can endow the protein with novel functions. In this light, we note that a mutant form of Doc2β, in which six Ca^{2+} ligands were neutralized, was found to rescue the loss of spontaneous SV release (minis) in Doc2α,β,γ/rabphilin quadruple-knockdown (KD) neurons (32). The authors concluded that Doc2β is not a Ca^{2+} sensor that regulates minis. However, the mutant form of Doc2β used in this study included neutralization of D220, which, again, causes the constitutive activation of the protein, in addition to endowing it with novel functions (16). Therefore it cannot be concluded from these experiments that Doc2β is not a Ca^{2+} sensor for spontaneous release. We also note that it is apparent that yet another sensor can couple Ca^{2+} to slow transmission, because syt1-KO/Doc2-KD nerve terminals respond, to a limited extent, to increases in $[Ca^{2+}]_i$ (15). In this model, the quadruple Doc2β Ca^{2+}-ligand mutant—which, again, fails to bind Ca^{2+} (16)—strongly enhances release regulated by another slow sensor.

In marked contrast to C2A, individual substitutions of three of the five acidic Ca^{2+} ligands in the C2B domain (D297N, D303N, and D357N) abolished Ca^{2+}-dependent translocation in PC12 cells, consistent with earlier work showing this domain is necessary and sufficient for translocation (23, 27). Moreover, these same mutants, D297,303N and D303N, also failed to enhance asynchronous release when expressed in neurons. We note that the D357,359N double mutant was able to translocate to the plasma membrane efficiently upon Ca^{2+} influx (Fig. 1 *B* and *C*); however, the D357N single ligand mutation eliminated the Ca^{2+}-dependent translocation activity of Doc2β (Fig. 2 *A* and *B*). Apparently, neutralization of the acidic residue at position 359 restored the ability of the D357N mutant to translocate and drive asynchronous release.

Kinetics of syt1–Doc2β Chimeras and the Rate of Vesicle Release. The kinetics of synaptic transmission play a crucial role in regulating and integrating signals in neuronal networks. For example, the kinetics of SV release determine, in part, the postsynaptic "spiking window" in magnocellular neurosecretory cells in the paraventricular nucleus of the hypothalamus (33) and play a critical role in the persistent reverberatory activity of neuronal networks formed by cultured hippocampal neurons (15, 34). The data presented here provide strong support for the hypothesis that Doc2β affects the kinetics of synaptic transmission by acting as a Ca^{2+} sensor for the slow phase of neurotransmitter release. Moreover, Doc2β and syt1 are both composed largely of tandem C2 domains, making it possible to generate chimeric sensors with intermediate intrinsic kinetic properties, potentially to alter network function.

Upon binding Ca^{2+}, Doc2β and syt1 operate, at least in part, by interacting with membranes that harbor negatively charged phospholipids (15, 30). The rate at which Ca^{2+}•sensor•liposome complexes disassemble upon rapid mixing with a Ca^{2+} chelator differs by >100-fold between Doc2β and syt1 (11, 15). This dramatic difference was used to screen a series of chimeras to identify the structural elements that underlie their distinct kinetics. Chimeras were generated between syt1 and Doc2β by swapping entire C2 domains (DASB and SADB) or individual loops (DL1–DL6) (Fig. 3). Exchanging individual loops in the C2A domain of syt1 had no effect on membrane disassembly or EPSC decay kinetics (Figs. 3 and 6). In contrast, replacing two loops in the C2B domain of syt1 with the corresponding loops of Doc2β (DL4 and DL6) resulted in chimeras with significantly slower membrane disassembly kinetics in vitro (DL6, 10-fold

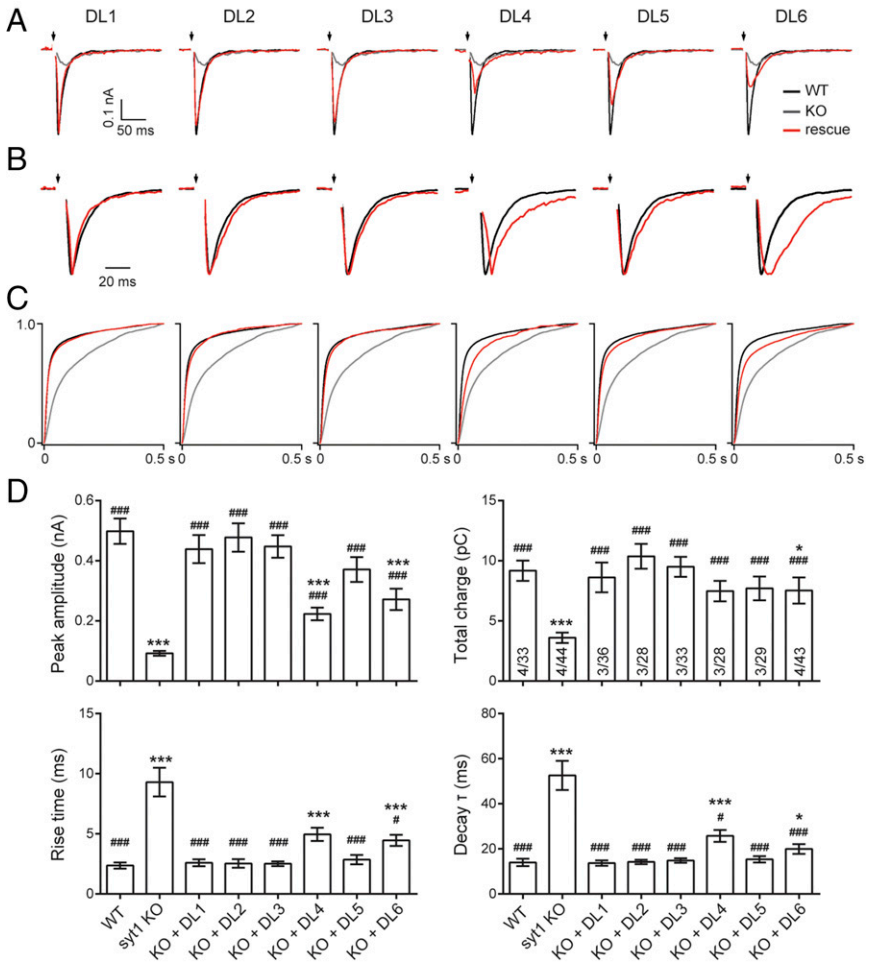

Fig. 6. Grafting individual Ca^{2+}-binding loops from the C2B domain of Doc2β onto syt1 slows EPSC kinetics. (*A*) Averaged evoked EPSCs recorded from WT neurons (black traces), syt1-KO neurons (gray traces), and syt1-KO neurons expressing WT syt1 or the loop-swap syt1–Doc2β chimeras (red traces). (*B*) The traces were normalized to peak values. (*C*) The cumulative charge transfer for each condition was calculated. (*D*) The kinetic components were analyzed using the parameters in Fig. 5. Grafting Doc2β loop 4 (t_{rise} = 4.96 ± 0.55 ms, τ_{decay} = 25.75 ± 2.64 ms, n = 28) or loop 6 (t_{rise} = 4.45 ± 0.46 ms, τ_{decay} = 19.95 ± 2.16 ms, n = 43) onto syt1 resulted in intermediate kinetics compared with WT and syt1-KO neurons; replacing the other syt1 loops with analogous loops from Doc2β had no effect. Data are presented as mean ± SEM; $^{*}P < 0.05$, $^{***}P < 0.001$ vs. WT, $^{\#}P < 0.05$, $^{\#\#\#}P < 0.001$ vs. syt1-KO, Kruskal–Wallis test followed by Dunn's post hoc test. The number of animals, *N*, and cells, *n*, are indicated in the bar graph as *N*/*n*.

slower; DL4, 20% slower). When expressed in syt1-KO neurons, these chimeras also yielded EPSCs with slow decay kinetics (Figs. 3 and 6). These experiments highlight the idea that C2B of both Doc2 and syt1 is the crucial domain that largely determines the properties of each protein. However, exchanging entire C2 domains (i.e., SADB and DASB) resulted in chimeras with intermediate lipid disassembly kinetics as compared with WT syt1 and Doc2β. When expressed in syt1-KO neurons, these two constructs also drove synaptic transmission with intermediate kinetics, although tm-SADB did give rise to slower decays compared with tm-DASB. Thus, additional structural elements might contribute, to some extent, to the kinetics of these sensors. It also is possible that inter–C2-domain interactions, which have been established for WT syt1 (31), impact the kinetics of the chimeras in complicated ways. Nevertheless, the emerging view, based on Ca^{2+}-ligand mutations and loop-swaps, is that the C2B domain of Doc2β is the primary element that determines translocation activity, as well as the time course of asynchronous transmission.

The syt1–Doc2β chimeras that slow release kinetics also increase the paired-pulse ratio (PPR) (Fig. S10). This phenotype is similar to a syt2 mutant that disrupts Ca^{2+} channel coupling (35). Therefore, both mechanisms—slower intrinsic kinetics and impaired coupling to Ca^{2+} channels—might underlie the slow kinetics of a synaptic transmission observed using the chimeras. We favor the former interpretation, because most of the chimeras studied possess intact Ca^{2+} channel-binding sites (36, 37) and because there is a qualitative correlation between the kinetics of the chimeras, as determined in vitro, with the time course of asynchronous transmission. Nonetheless, flash photolysis of caged-Ca^{2+}, to bypass Ca^{2+} channels (38), might help discriminate between these two mechanisms.

In summary, the data reported here, obtained using a combination of biochemical, biophysical, and electrophysiological approaches, provide direct evidence that Doc2β must bind Ca^{2+} and translocate to the plasma membrane, via Ca^{2+}- and membrane-binding loops in the C2B domain, to enhance asynchronous synaptic transmission. Mechanistically, it appears that the C2B domain of Doc2β first senses Ca^{2+} to drive translocation to the plasma membrane, where C2A then is able to bind Ca^{2+} because of the presence of acidic phospholipids (16). We assume that both C2 domains then partially insert into the plasma membrane, as has been shown for syt1 (29, 31, 39, 40), to drive lipid rearrangements that accelerate SNARE catalyzed fusion. These rearrangements include the putative bending of the target

membrane (41, 42) and/or the close juxtaposition of the bilayers, allowing them to fuse (39). Thus, it will be important to determine whether the C2 domains of Doc2 do in fact insert into membranes and to determine more precisely how this interaction regulates fusion.

Materials and Methods

Molecular Biology. The pGEX4T vector encoding the tandem C2 domains (C2AB) of rat Doc2β (amino acids125–412) was provided by M. Verhage, University of Amsterdam, Amsterdam. A cDNA encoding the N-terminal domain of rat Doc2β (amino acids 1–124) was synthesized and recoded to reduce guanine and cytosine content (Integrated DNA Technologies). The recoded fragment was annealed to cDNA encoding the C2AB domain to generate full-length Doc2β constructs. The Ca^{2+}-ligand mutations in Doc2β were generated using a QuikChange site-specific mutagenesis kit (Agilent Technologies). For expression in mammalian cells, the same mutations were introduced into full-length Doc2β (that had been built by ligating the recoded N-terminal domain to the C2AB domain) and were subcloned into pAcGFP1-C1 to generate N-terminal GFP fusion proteins or into pLOX [Syn-DsRed(W)-Syn-GFP(W)] to generate lentiviral particles. cDNA encoding rat syt1 was provided by T. C. Sudhof, Stanford University, Stanford, CA; the D374 mutation was corrected, as described previously (43). The C2AB fragment (amino acids 96–421) of syt1 was expressed as a GST fusion protein using pGEX4T as described (44).

The syt1–Doc2β chimeras SADB (syt1 amino acids 96–272; Doc2β amino acids 259–412), DASB (Doc2β amino acids 125–258; syt1 amino acids 273–421), tm-SADB (syt1 amino acids 1–272; Doc2β amino acids 259–412), tm-DASB (syt1 amino acids 1–139; Doc2β amino acids 125–258; syt1 amino acids 273–421), and tm-Doc2β (syt1 amino acids 1–139; Doc2β amino acids 125–421) were generated using splicing by overlap extension PCR. The individual loops of full-length syt1, as well as the C2AB fragment, were replaced with the corresponding loops of Doc2β using the overlapping primer method. The syt1 sequence was modified as follows: DL1 (syt1 loop 1, ELPALDMGGTSD was changed to GLKPMDHNGLAD), DL2 (syt1 loop 2, ETKVHRKTLNP was changed to RTKTLRNTLNP), DL3 (syt1 loop 3, DFDRFSKHD was changed to DEDKFRHNE), DL4 (syt1 loop 4, KNLKKMDVGGLSD was changed to AHLAAMDANGYSDP), DL5 (syt1 loop 5, KTTIKKNTLNP was changed to KTAVKKKTLNP), DL6 (syt1 loop 6, VLDYDKIGKNDA was changed to VWDYDIGKSND). A bacterial expression vector to generate the syntaxin 1A and SNAP-25B heterodimer (pTW34) was provided by J. E. Rothman, Yale University, New Haven, CT.

Protein Purification and Liposome Preparation. The preassembled t-SNARE heterodimer, composed of full-length syntaxin 1A and SNAP-25B, was purified and reconstituted as described previously (45). The C2AB fragments of syt1, Doc2β, or the chimeras were expressed as GST-fusion proteins and purified using standard procedures as described previously (16). Proteins were separated by SDS/PAGE and stained with Coomassie blue; concentrations were determined using a BSA standard curve.

Liposome Preparation and Binding Assays. Liposomes [25% phosphatidylserine (PS), 30% phosphatidylethanolamine (PE), and 45% phosphatidylcholine (PC) (mol/mol)] were prepared as described previously (11). For stopped-flow experiments, 5% Dansyl-PE (mol/mol) was substituted into the liposomes, and the PE was maintained at 30% (mol/mol). Briefly, lipids stored in chloroform were aliquoted into a glass test tube and dried under a stream of nitrogen. Dried lipids were lyophilized for at least 1 h to remove residual solvent. The lipid film was resuspended at 20 mM in reconstitution buffer [25 mM Hepes-KOH (pH 7.4), 100 mM KCl, 10% (wt/vol) glycerol, 1 mM DTT] and extruded 29 times through a 100-nm filter (Avanti Polar Lipids).

Cosedimentation experiments were performed as described previously (16). Briefly, 100-μL reactions containing 4 μM protein, liposomes (4 mM lipid), and increasing amounts of Ca^{2+} were prepared in reconstitution buffer lacking glycerol. Samples were incubated for 15 min at RT with shaking and were centrifuged at 65,000 rpm using a TLA100 rotor (Beckman) for 30 min; 60 μL of the supernatant from each sample was collected and mixed with 30 μL of 3× SDS sample buffer [120 mM Tris·HCl (pH 6.8), 30% (wt/vol) glycerol, 15 mM TCEP, and 125 mM SDS]. Samples were boiled for 1 min, and 15-μL aliquots were analyzed by SDS/PAGE and stained with Coomassie blue.

For coflotation assays, 100-μL reactions containing 0.2 mM EGTA, 30 μM protein, and 45 μL PS-free t-SNARE–bearing or protein-free vesicles were prepared in reconstitution buffer. Samples were incubated for 30 min at RT with shaking followed by flotation through a density gradient in the presence of 1 mM free Ca^{2+} or 0.2 mM EGTA. Vesicles were collected and resolved by SDS/PAGE; gels were stained with Coomassie blue.

Stopped-Flow Rapid-Mixing Experiments. Kinetics experiments were performed using an SX.18MV stopped-flow spectrometer (Applied Photophysics) at 15 °C as described previously (11), with liposomes composed of 25% PS, 25% PE, 45% PC, and 5% dansyl-PE (mol/mol). For liposome disassembly experiments, liposomes (4 mM lipid), 0.2 mM Ca^{2+}, and 4 μM protein in one syringe were mixed rapidly with 5 mM EGTA in a 1:1 ratio. FRET was monitored by exciting aromatic residues at 280 nm and monitoring the emission of the dansyl acceptor via a 520/35 nm band-pass filter. All data points are the average of three independent experiments in which five or more separate traces were averaged for each experiment.

Hippocampal Neuronal Culture and Viral Infection. Hippocampal neuronal cultures were prepared from syt1-KO mice (Jackson Laboratory) or their WT littermates at postnatal day 0, in accordance with the guidelines of the National Institutes of Health (46), as approved by the Animal Care and Use Committee at the University of Wisconsin, as described previously (7). Briefly, hippocampi were isolated from mouse brain, washed with HBSS (Corning), digested for 30 min at 37 °C in 0.25% Trypsin-EDTA (Corning), and mechanically dissociated. The dissociated neurons were plated at ∼25,000–40,000 cells/cm^2 on poly-D-lysine (Life Technologies)-coated 12 mm glass coverslips (Warner Instruments) and were cultured in Neurobasal-A medium supplemented with B27 and GlutaMAX (Life Technologies), maintained at 37 °C in a 5% CO_2 humidified incubator.

cDNA constructs encoding full-length WT syt1, WT Doc2β, Doc2β mutants, and syt1–Doc2β chimeras were subcloned into the pLOX vector and transfected into HEK 293T cells, together with two viral packaging vectors (vesicular stomatitis virus G glycoprotein and Delta 8.9), to generate lentiviral particles. Three days posttransfection, virus particles were harvested from HEK 293T cells by centrifugation for 2 h at 25,000 rpm using a SW28 rotor (Beckman). Cultures were infected with virus at 5 d in vitro (DIV). The infection rate was ∼90% as determined by the coexpression of GFP in the pLOX vector.

Translocation Assays. Translocation assays were performed as previously described (16). Briefly, PC12 cells were cultured in 24-well dishes on glass coverslips coated with poly-D-lysine and collagen IV. When PC12 cells reached ∼70–80% confluency, they were transfected with 0.5 μg of DNA using Lipofectamine LTX reagent (Life Technologies). Primary hippocampal neurons were transfected using a Ca^{2+} Phosphate Transfection Kit (Life Technologies) at ∼7–10 DIV. Twenty-four to forty-eight hours after transfection, coverslips were transferred to 30-mm culture dishes containing 2 mL of imaging buffer [145 mM NaCl, 2.8 mM KCl, 1 mM $MgCl_2$, 1.2 mM $CaCl_2$, 10 mM glucose, and 10 mM Hepes-NaOH (pH 7.3)]. Individual cells were imaged using an Olympus FV1000 confocal microscope before and after the addition of 2 mL of depolarization buffer [27.8 mM NaCl, 120 mM KCl, 1mM $MgCl_2$, 1.2 mM $CaCl_2$, 10 mM glucose, and 10 mM Hepes-NaOH (pH 7.3)] to monitor the cellular localization of the GFP-tagged protein. Line scan analysis was performed on individual cells before and after treatment with KCl using ImageJ 10.2 software (NIH).

Immunocytochemistry. At ∼13–15 DIV, neurons were fixed for 15 min with 4% paraformaldehyde (wt/vol) in PBS, permeabilized for 10 min in 0.1% Triton X-100 (vol/vol), and blocked for 30 min with 10% BSA (wt/vol) plus 0.1% Triton X-100 (vol/vol). Coverslips then were incubated with primary antibodies at RT for 2 h. A monoclonal mouse antibody that recognizes the luminal domain of syt1, 604.1 (SYnaptic SYstems; 1:1,000 dilution) (47), was used to determine the localization of the syt1–Doc2β chimeras. Nerve terminals were identified using a polyclonal guinea pig anti-synaptophysin antibody (SYnaptic SYstems; 1:1,000 dilution). Samples were washed with PBS three times and then were stained with Alexa 488-tagged anti-mouse (1:500 dilution), and Alexa 594-tagged anti-guinea pig (1:500 dilution) secondary antibodies (Jackson ImmunoResearch Laboratories) for 1 h. Coverslips were washed three times with PBS and mounted in Fluoromount (Southern Biotechnology Associates). Images were acquired using an Olympus FV1000 upright confocal microscope with a 60× 1.40NA oil objective under identical laser and gain settings for all samples. To quantify the colocalization of syt1 or syt1–Doc2β chimeras with synaptophysin, the Mander's coefficient of each image was calculated using ImageJ 10.2 software with the JACoP plug-in (48).

Immunoblot Analysis. Cultured neurons were solubilized in lysis buffer [20 mM Tris, 150 mM NaCl, 1% Triton X-100, 0.05% SDS, 0.5% PMSF, 0.5 mg/mL leupeptin, 0.7 mg/mL pepstatin, 1mg/mL aprotinin (pH 7.4)] at ∼13–15 DIV. The lysates were centrifuged for 10 min at 13,400 × *g* at 4 °C. Supernatants were subjected to SDS/PAGE and immunoblotted using the anti-syt1 mouse monoclonal antibody 604.1 (1:1,000 dilution); blots also were probed with a mouse polyclonal antibody against valosin-containing protein (VCP) (Abcam; 1:800

dilution) as a loading control. Immunoreactive bands were detected using an HRP-conjugated anti-mouse secondary antibody (Abcam; 1:2,000 dilution).

Electrophysiology. Hippocampal neurons were whole-cell patch-clamped at ~13–17 DIV. During recordings, neurons were perfused continuously with bath solution [128 mM NaCl, 30 mM glucose, 5 mM KCl, 5 mM $CaCl_2$, 1 mM $MgCl_2$, 50 mM D-AP5, 20 mM bicuculline, and 25 mM Hepes (pH 7.3)]. The recording pipettes were pulled from glass capillary tubes (Warner Instruments) and filled with pipette solution [130 mM K-gluconate, 1 mM EGTA, 5 mM Na-phosphocreatine, 2 mM Mg-ATP, 0.3 mM Na-GTP, 5 mM QX-314, and 10 mM Hepes (pH 7.3)]. Neurons were voltage clamped at −70 mV using a MultiClamp 700B amplifier (Molecular Devices) or an EPC-10 double amplifier (HEKA Elektronik). Only whole-cell patches with series resistances <15 MΩ were used for recording. D-AP5, bicuculline, and QX-314 were from TOCRIS Bioscience; other chemicals were from Sigma-Aldrich.

For evoked EPSCs, the presynaptic neuron was stimulated by a voltage step (40 V, 1 ms) delivered via a bipolar electrode pulled from theta tubing (Warner Instruments) and filled with bath solution. For the RRP measurements, the release of RRP was driven by local perfusion of bath solution plus 500 mM sucrose, using a Picospritzer III (Parker). For mEPSC recordings, 1 μM tetrodotoxin (TOCRIS Bioscience) was added to the bath solution. For evoked EPSC recordings under physiological conditions, the $CaCl_2$ concentration in bath solution was reduced to 1.2 mM, and neurons were maintained at 35 °C using a heated in-line perfusion tube (ALA Scientific Instruments) during the recordings. All other electrophysiology recordings were performed at RT. All data were acquired using pClamp (Molecular Devices) or PatchMaster (HEKA Elektronik) software, digitized at 10 kHz, and filtered at 2.8 kHz. Recorded traces were analyzed using Clampfit (Molecular Devices) and Igor (WaveMetrics) software.

ACKNOWLEDGMENTS. We thank X. Lou and members of the E.R.C. laboratory for critical comments regarding this manuscript. This study was supported by NIH Grant MH 61876. E.R.C. is an Investigator of the Howard Hughes Medical Institute.

1. Koh TW, Bellen HJ (2003) Synaptotagmin I, a Ca2+ sensor for neurotransmitter release. *Trends Neurosci* 26(8):413–422.
2. Chapman ER (2002) Synaptotagmin: A Ca(2+) sensor that triggers exocytosis? *Nat Rev Mol Cell Biol* 3(7):498–508.
3. Littleton JT, Stern M, Schulze K, Perin M, Bellen HJ (1993) Mutational analysis of Drosophila synaptotagmin demonstrates its essential role in Ca(2+)-activated neurotransmitter release. *Cell* 74(6):1125–1134.
4. Broadie K, Bellen HJ, DiAntonio A, Littleton JT, Schwarz TL (1994) Absence of synaptotagmin disrupts excitation-secretion coupling during synaptic transmission. *Proc Natl Acad Sci USA* 91(22):10727–10731.
5. Geppert M, et al. (1994) Synaptotagmin I: A major Ca2+ sensor for transmitter release at a central synapse. *Cell* 79(4):717–727.
6. Nishiki T, Augustine GJ (2004) Dual roles of the C2B domain of synaptotagmin I in synchronizing Ca2+-dependent neurotransmitter release. *J Neurosci* 24(39): 8542–8550.
7. Liu H, Dean C, Arthur CP, Dong M, Chapman ER (2009) Autapses and networks of hippocampal neurons exhibit distinct synaptic transmission phenotypes in the absence of synaptotagmin I. *J Neurosci* 29(23):7395–7403.
8. Raingo J, et al. (2012) VAMP4 directs synaptic vesicles to a pool that selectively maintains asynchronous neurotransmission. *Nat Neurosci* 15(5):738–745.
9. Hu Z, Tong XJ, Kaplan JM (2013) UNC-13L, UNC-13S, and Tomosyn form a protein code for fast and slow neurotransmitter release in Caenorhabditis elegans. *eLife* 2:e00967.
10. Bacaj T, et al. (2013) Synaptotagmin-1 and synaptotagmin-7 trigger synchronous and asynchronous phases of neurotransmitter release. *Neuron* 80(4):947–959.
11. Hui E, et al. (2005) Three distinct kinetic groupings of the synaptotagmin family: Candidate sensors for rapid and delayed exocytosis. *Proc Natl Acad Sci USA* 102(14): 5210–5214.
12. Maximov A, et al. (2008) Genetic analysis of synaptotagmin-7 function in synaptic vesicle exocytosis. *Proc Natl Acad Sci USA* 105(10):3986–3991.
13. Liu H, et al. (2014) Synaptotagmin 7 functions as a Ca2+-sensor for synaptic vesicle replenishment. *eLife* 3:e01524.
14. Weber JP, Toft-Bertelsen TL, Mohrmann R, Delgado-Martinez I, Sørensen JB (2014) Synaptotagmin-7 is an asynchronous calcium sensor for synaptic transmission in neurons expressing SNAP-23. *PLoS One* 9(11):e114033.
15. Yao J, Gaffaney JD, Kwon SE, Chapman ER (2011) Doc2 is a Ca2+ sensor required for asynchronous neurotransmitter release. *Cell* 147(3):666–677.
16. Gaffaney JD, Xue R, Chapman ER (2014) Mutations that disrupt Ca^{2+}-binding activity endow Doc2β with novel functional properties during synaptic transmission. *Mol Biol Cell* 25(4):481–494.
17. Sakaguchi G, Orita S, Maeda M, Igarashi H, Takai Y (1995) Molecular cloning of an isoform of Doc2 having two C2-like domains. *Biochem Biophys Res Commun* 217(3): 1053–1061.
18. Kojima T, Fukuda M, Aruga J, Mikoshiba K (1996) Calcium-dependent phospholipid binding to the C2A domain of a ubiquitous form of double C2 protein (Doc2 beta). *J Biochem* 120(3):671–676.
19. Fukuda M, Mikoshiba K (2000) Doc2gamma, a third isoform of double C2 protein, lacking calcium-dependent phospholipid binding activity. *Biochem Biophys Res Commun* 276(2):626–632.
20. Groffen AJA, et al. (2004) Ca(2+)-induced recruitment of the secretory vesicle protein DOC2B to the target membrane. *J Biol Chem* 279(22):23740–23747.
21. Groffen AJA, Friedrich R, Brian EC, Ashery U, Verhage M (2006) DOC2A and DOC2B are sensors for neuronal activity with unique calcium-dependent and kinetic properties. *J Neurochem* 97(3):818–833.
22. Miyazaki M, et al. (2009) DOC2b is a SNARE regulator of glucose-stimulated delayed insulin secretion. *Biochem Biophys Res Commun* 384(4):461–465.
23. Fukuda N, et al. (2009) DOC2B: A novel syntaxin-4 binding protein mediating insulin-regulated GLUT4 vesicle fusion in adipocytes. *Diabetes* 58(2):377–384.
24. Friedrich R, et al. (2008) DOC2B acts as a calcium switch and enhances vesicle fusion. *J Neurosci* 28(27):6794–6806.
25. Groffen AJ, et al. (2010) Doc2b is a high-affinity Ca2+ sensor for spontaneous neurotransmitter release. *Science* 327(5973):1614–1618.
26. Yu H, Rathore SS, Davis EM, Ouyang Y, Shen J (2013) Doc2b promotes GLUT4 exocytosis by activating the SNARE-mediated fusion reaction in a calcium- and membrane bending-dependent manner. *Mol Biol Cell* 24(8):1176–1184.
27. Giladi M, et al. (2013) The C2B domain is the primary Ca2+ sensor in DOC2B: A structural and functional analysis. *J Mol Biol* 425(22):4629–4641.
28. Earles CA, Bai J, Wang P, Chapman ER (2001) The tandem C2 domains of synaptotagmin contain redundant Ca2+ binding sites that cooperate to engage t-SNAREs and trigger exocytosis. *J Cell Biol* 154(6):1117–1123.
29. Bai J, Wang P, Chapman ER (2002) C2A activates a cryptic Ca(2+)-triggered membrane penetration activity within the C2B domain of synaptotagmin I. *Proc Natl Acad Sci USA* 99(3):1665–1670.
30. Bhalla A, Tucker WC, Chapman ER (2005) Synaptotagmin isoforms couple distinct ranges of Ca2+, Ba2+, and Sr2+ concentration to SNARE-mediated membrane fusion. *Mol Biol Cell* 16(10):4755–4764.
31. Liu H, et al. (2014) Linker mutations reveal the complexity of synaptotagmin 1 action during synaptic transmission. *Nat Neurosci* 17(5):670–677.
32. Pang ZPP, et al. (2011) Doc2 supports spontaneous synaptic transmission by a Ca(2+)-independent mechanism. *Neuron* 70(2):244–251.
33. Iremonger KJ, Bains JS (2007) Integration of asynchronously released quanta prolongs the postsynaptic spike window. *J Neurosci* 27(25):6684–6691.
34. Lau PM, Bi GQ (2005) Synaptic mechanisms of persistent reverberatory activity in neuronal networks. *Proc Natl Acad Sci USA* 102(29):10333–10338.
35. Young SM, Jr, Neher E (2009) Synaptotagmin has an essential function in synaptic vesicle positioning for synchronous release in addition to its role as a calcium sensor. *Neuron* 63(4):482–496.
36. Sheng ZH, Yokoyama CT, Catterall WA (1997) Interaction of the synprint site of N-type Ca2+ channels with the C2B domain of synaptotagmin I. *Proc Natl Acad Sci USA* 94(10):5405–5410.
37. Chapman ER, Desai RC, Davis AF, Tornehl CK (1998) Delineation of the oligomerization, AP-2 binding, and synprint binding region of the C2B domain of synaptotagmin. *J Biol Chem* 273(49):32966–32972.
38. Burgalossi A, et al. (2010) SNARE protein recycling by αSNAP and βSNAP supports synaptic vesicle priming. *Neuron* 68(3):473–487.
39. Hui E, et al. (2011) Mechanism and function of synaptotagmin-mediated membrane apposition. *Nat Struct Mol Biol* 18(7):813–821.
40. Paddock BE, et al. (2011) Membrane penetration by synaptotagmin is required for coupling calcium binding to vesicle fusion in vivo. *J Neurosci* 31(6):2248–2257.
41. Martens S, Kozlov MM, McMahon HT (2007) How synaptotagmin promotes membrane fusion. *Science* 316(5828):1205–1208.
42. Hui E, Johnson CP, Yao J, Dunning FM, Chapman ER (2009) Synaptotagmin-mediated bending of the target membrane is a critical step in Ca(2+)-regulated fusion. *Cell* 138(4):709–721.
43. Desai RC, et al. (2000) The C2B domain of synaptotagmin is a Ca(2+)-sensing module essential for exocytosis. *J Cell Biol* 150(5):1125–1136.
44. Tucker WC, et al. (2003) Identification of synaptotagmin effectors via acute inhibition of secretion from cracked PC12 cells. *J Cell Biol* 162(2):199–209.
45. Tucker WC, Weber T, Chapman ER (2004) Reconstitution of Ca2+-regulated membrane fusion by synaptotagmin and SNAREs. *Science* 304(5669):435–438.
46. Committee on Care and Use of Laboratory Animals (1996) *Guide for the Care and Use of Laboratory Animals* (Natl Inst Health, Bethesda), DHHS Publ No (NIH) 85-23.
47. Chapman ER, Jahn R (1994) Calcium-dependent interaction of the cytoplasmic region of synaptotagmin with membranes. Autonomous function of a single C2-homologous domain. *J Biol Chem* 269(8):5735–5741.
48. Bolte S, Cordelieres FP (2006) A guided tour into subcellular colocalization analysis in light microscopy. *J Microsc* 224(pt3):213–232.